RESEARCH ARTICLE | NOVEMBER 07 2023

Deep trap assisting elastico-mechanoluminescence in diphase non-piezoelectrics induced by tunneling effect

Yin Li ; Zishuo Li ; Hailing Sun ; K. W. Kwok ; Guofu Zhou

Appl. Phys. Lett. 123, 192902 (2023)
https://doi.org/10.1063/5.0170880

Applied Physics Letters ARTICLE pubs.aip.org/aip/apl

Deep trap assisting elastico-mechanoluminescence in diphase non-piezoelectrics induced by tunneling effect

Cite as: Appl. Phys. Lett. **123**, 192902 (2023); doi: 10.1063/5.0170880
Submitted: 5 August 2023 · Accepted: 12 October 2023 ·
Published Online: 7 November 2023

Yin Li,[1,2] Zishuo Li,[1] Hailing Sun,[1,2,a)] K. W. Kwok,[2,a)] and Guofu Zhou[1]

AFFILIATIONS

[1]Guangdong Provincial Key Laboratory of Optical Information Materials and Technology & Institute of Electronic Paper Displays, South China Academy of Advanced Optoelectronics, South China Normal University, Guangzhou 510006, China
[2]Department of Applied Physics, The Hong Kong Polytechnic University, Kowloon, Hong Kong

[a)]**Authors to whom correspondence should be addressed:** hailing.sun@m.scnu.edu.cn and apkwkwok@polyu.edu.hk

ABSTRACT

The sustainable conversion of mechanical energy into light (elastico-mechanoluminescence, EML) opens up possibilities for energy-saving, which is of pivotal significance in addressing the energy crisis. The concepts of piezophotonics and the piezoelectric field's dependence on the probability of charge carriers detrapping have been thoroughly developed in explaining EML. Nevertheless, in contrast to the EML triggered by the piezoelectricity model, strong elastico-mechanoluminescence phenomena have also been frequently discovered in non-piezoelectric materials. Is the working principle different? This paper provides physical insight into the reconfigurable EML phenomena of intrinsic non-piezoelectric systems. It emphasizes the exploration of the mechanism through comprehensive analysis of trap information, de-trapping processes, and the lifetime of charge carriers in traps. We demonstrate the assistance of deep trap to enhance the red EML mode in a diphase centrosymmetric luminescent host through the electron tunneling effect. This advancement supports the progress of non-piezoelectric EML dielectrics and offers an appealing alternative approach in this field.

Elastico-mechanoluminescence (EML) contributes to the photon emission triggered by environmental mechanical stimulation in a reproducible and non-destructive way. Therefore, it has great potential in practical applications, such as stress sensors, bioimaging, engineering structure detection, and energy technology.[1–9] Since the discovery of ZnS:Mn^{2+} and $SrAl_2O_4$ Eu^{2+} in 1999,[10,11] many EML materials, which consist of luminescent dopant ions and host matrix, have been developed. The host matrix can be dielectric oxides or II–VI semiconductors, while the dopant ions are mostly rare-earth element or transition metal ions. Their combination brings various EML colors, such as $SrAl_2O_4$:Eu^{2+} (greenish-blue),[11] $mCaO{\cdot}Nb_2O_5$:Pr^{3+} (red),[12] ZnS:Mn^{2+} (orange),[1] ZnS:Cu (greenish-blue),[13] and ZnS/CaZnOS:Mn^{2+}/Ln^{3+} (full spectrum).[14] As one of the most reliable EML materials, ZnS:metal has been thoroughly studied, and a widely accepted piezoelectricity-induced EML model was developed to describe its working principle. Considering the nature of those known EML materials, this model generally requires long-lived charge carrier traps to store energy and a piezoelectric field induced by mechanical stimulus to release the trapped charge carriers.[1,15–17] The released free charge carriers transfer to the position of luminescent centers (dopant ions) and subsequently induce the emission of photons. Based on this model, many scientists have been exploring EML materials by screening the piezoelectric materials, which also exhibit trap-controlled luminescence (i.e., persistent luminescence).[7,9,18,19] Therefore, it is necessary to have a comprehensive understanding of the function of traps when conducting research on EML materials.

Many scholars have revealed the strong correlation between traps and EML intensity,[16–18,20–22] and the traps participating in EML are generally created during the synthesis of materials from three main sources. Case I: When the charges of dopant ions deviate from those of the host metal ions they substitute, non-equivalent substitution occurs. Then electron/hole traps are produced according to the charge difference between the dopant ions and host metal ions. For example, when divalent calcium ions (Ca^{2+}) are replaced by trivalent praseodymium (Pr^{3+}), the defects $Pr_{Ca}^{\cdot}$ carrying one positive charge are produced, which are correspondingly classified as electron traps. Due to charge compensation, cation vacancies V_{Ca}'' carrying two negative charges are also generated simultaneously and work as hole traps. Case II:

When the dopant ions have the same charges as the host metal ions, the difference in electronegativity and ion radius between the dopant ions and host ions generates isoelectronic traps, which usually occur in semiconductors, like ZnS:metal. Case III: Except for traps originating from luminescent doping, there are other types of traps resulting from element deficiency. Taking dielectric oxides as an example, oxygen vacancies are created when the materials are sintered in a reducing atmosphere, while cation vacancies are created when sintered in an oxidant atmosphere. In addition, traps can also be created by adjusting the stoichiometry of the composing elements, including the sublimation of reactants during solid-state reactions and cation exchange between different lattice sites. More relevantly, the identification of traps in materials can be based on thermoluminescence (TL) to indicate the number of trap types, energy levels of traps, and concentrations of traps.[18,21,23] Also, the persistent luminescence (PsL) phenomenon also has a close relationship with long-lived trap levels for energy storage, and thus, persistent phosphors are considered as candidates for EML materials.[24–27]

However, the mechanism underlying de-trapping of trapped charge carriers during elastico-mechanoluminescence is mysterious. Assumption I: piezoelectricity-induced EML model. Since the mechanical energy produced by an external force (10^{-6}–10^{-5} eV)[28] is far less than the trap depth in EML materials ($\sim 10^{-1}$ eV); therefore, there are supposed to other ways for the mechanical load to release the charge carriers. Many scholars have attributed this to the internal piezoelectric field caused by deformation of the host matrix, and the working principle of most EML materials could be well explained in this way. Thus, piezoelectricity is considered as an indispensable part of EML.[15–17,29,30] Assumption II: What kind of non-piezoelectric EML model? Since Zhao *et al.* reported that $CaTiO_3:Pr^{3+}$, which is known as non-piezoelectric, can also emit strong red light under elastic deformation,[31] EML phenomena in non-piezoelectric materials have been frequently discovered in recent years.[32–35] However, how does the EML work in these non-piezoelectrics? Although some propose a movement of dislocation mechanism for the occurrence of EML, while other assumptions indicate that electron tunneling, as well as the electric field (produced by domain structures), would induce EML, and this issue is still controversial and pending in non-piezoelectric EML systems.

In this paper, derived of typical centrosymmetric luminescent material $CaTiO_3:Pr^{3+}$, which serves as a red-light emitting phosphor with long-time afterglow decay,[12,31,32,36,37] and the classical piezoelectric host of $Ba_{0.85}Ca_{0.15}Ti_{0.9}Zr_{0.1}O_3$ (Refs. 38–40), we approach an equivalent substitution strategy of designing the non-piezoelectric host matrix as $Ca_{0.85}Ba_{0.15}Ti_{0.9}Zr_{0.1}O_3$:0.2%Pr by introducing the originated diphase structure. The mechanism underlying the de-trapping of trapped charge carriers will be comprehensively investigated, aiming to promote the development of non-piezoelectric EML materials and provide an alternative route beyond the current research direction.

To examine the non-piezoelectric feature of EML host, the crystal structure information of as-designed CBTZ:Pr sample was figured out by XRD [Fig. 1(a)]. After the Rietveld refinement (with a satisfying $R_{wp} = 9.85\%$), each characteristic peak of the experimental data can be recognized in composing phases, which confirms the coexistence of two phases in CBTZ:Pr. One is identified as having a cubic structure analogous to $BaZrO_3$ (COD ID: 1532743), while the other exhibits an orthorhombic structure similar to $CaTiO_3$ (COD ID: 1000022). Both

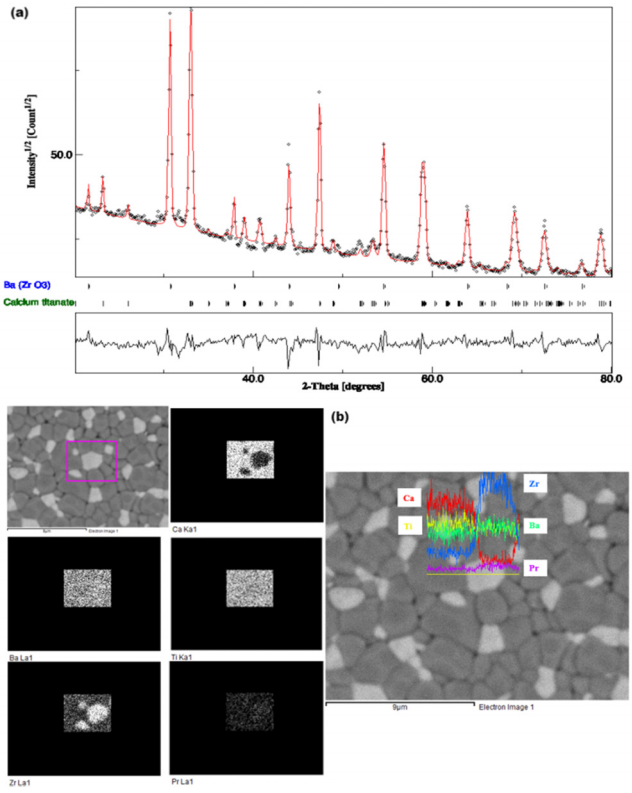

FIG. 1. (a) XRD pattern and Rietveld refinement and (b) BSE images and EDS element analyzation of CBTZ:Pr.

of the phases are structurally non-polar without containing a tetragonally piezoelectric phase. In accordance with this, the XRD pattern Rietveld refinement of CBT:Pr (Fig. S1) also identifies the non-piezoelectric $CaTiO_3$ centrosymmetric structure.

Results of the originally designed diphase microstructure and corresponding composition analyzation in the modified CBTZ:Pr are presented with back scattered electron (BSE) microscope images [Fig. 1(b)]. It can be interestingly observed that, consistent with the coexistence of two phases from XRD, the sample shows a bright phase and a dark phase with obvious boundaries separating each other under BSE. Revealed by energy dispersive spectrometer (EDS) element analysis, the brighter phase is comparatively rich in Zr and Ba elements, while the darker phase is relatively rich in Ca and Ti. This should correspond to $BaZrO_3$ and $CaTiO_3$, respectively, confirming the non-piezoelectric diphase microstructure obtained in modified CBTZ:Pr. By comparison, the $Ca_{0.9}Ba_{0.1}TiO_3$:0.2%Pr (abbreviated as CBT:Pr) samples show a uniform phase structure with a dark color [Fig. S2(b)], further supporting the XRD results in Fig. S1.

Before examining the EML behavior, we investigated the luminescent properties to gain a better understanding of the function of traps. As shown in Fig. 2(a), when exposed to UV light at 365 nm, the CBTZ:Pr sample exhibits the most intense red PL resulted from its abundant 4f level transitions, and the red emission remains detectable in 10 min duration after the UV irradiation stops. When comparing the thermoluminescence (TL) glow curve and EML spectra to the PL

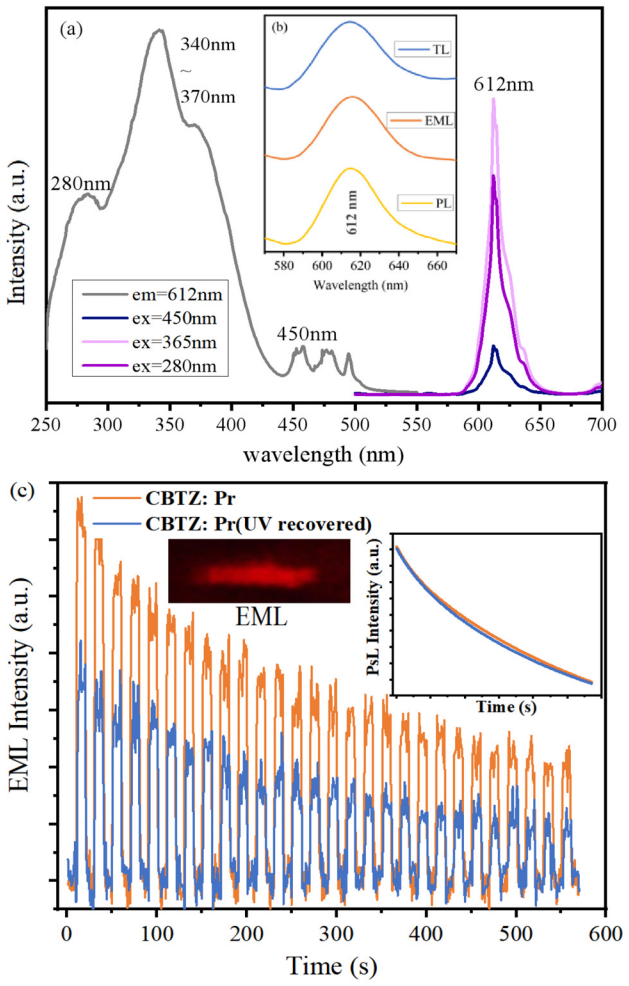

FIG. 2. (a) PL and PLE behaviors; (b) comparison of TL, EML and PL spectra; and (c) EML behavior under first UV irradiation and after re-irradiation during application of repetitive tensile load. Inset: the EML image and PsL decay curve for duration measurement.

behavior of CBTZ:Pr in Fig. 2(b), it can be observed that all of them exhibit a typical 612 nm emission. This indicates that the luminescent center of trivalent Pr undergoes the same $^1D_2 \rightarrow {}^3H_4$ transition during EML, TL, and PL processes, which is closely related to the inherited trap information in the rare-earth doped dielectric host. Further discussion on this mechanism model will be provided in the following paragraph.

For sustainable EML behavior measurement, the stripe shaped CBTZ:Pr/PDMS composite samples were subjected to a periodic tensile force of 2 Hz for ten seconds, with inactivity intervals of ten seconds. The force was applied using the blunt probe of an electromagnet controlled by an oscillator. As shown in Fig. 2(c), the EML emission keeps occurring periodically when the tensile force is repetitively applied and disappears immediately when the force stops in a collaborative response. The decay curve of persistent luminescence (PsL) is obtained by fitting the data points when no force is applied, revealing the PsL decay pattern during the EML measurement. After UV re-irradiation, the intensity of EML is partially recovered. Although the intensity is not as strong as in the first test, a similar EML pattern can still be observed when the repetitive tensile force is applied. More relevantly, the decay rate of EML intensity for UV recovered CBTZ:Pr is almost parallel to the original one while the fitted PsL curves of the two samples are almost overlap [inset plots of Fig. 2(c)]. The EML intensity reasonably degrades, which can be attributed to the irreversible deformation created in the soft PDMS matrix during the repetitive application of tensile force. Nevertheless, the complete recovery of persistent luminescence intensity demonstrates the presence of traps, highlighting the inherent potential in sustainable EML properties.

The sustainable EML behaviour, which can be recovered by UV exposure, indicates the noteworthy role of traps in the mechanism. As we know, thermal luminescence combined with fitting calculations is a well-known indirect method for effectively detecting trap defects. In order to explore the trap levels, the TL glow curve of CBTZ:Pr is investigated and resolved into multiple Gaussian-shaped peaks in Fig. 3. The activation energy (E) of the trap level in each peak could be estimated using the following equation:[23]

$$E = 2kT_m(1.26T_m/\omega - 1)\,, \tag{1}$$

where ω is the full width of half magnitude of the peak, k is the Boltzmann constant, and T_m is the temperature of the peak value. Derived from Eq. (1), the activation energy of trap corresponding to peak 1 in the TL glow curve is 0.70 eV, which is close to the optimal depth (~0.65 eV) reported for PsL emission.[41] The intensity of peak 1 is the highest among all peaks presented in the glow curve, indicating traps corresponding to peak 1 are supposed to store electrons with the highest concentration and accordingly dominate PsL process. In addition, the trap depth for peak 3 is 0.23 eV identified as shallow trap, and charge carriers in shallow trap are prone to full release around room temperature. The trap depth for peak 2 is 1.11 eV, with the value between the PsL trap and the deep trap (~2.0 eV).[25] Due to the relatively high value of activation energy, this trap hardly contributes to PsL/EML directly since it is unable to release the trapped charge carriers with ambient thermal energy or pure mechanical energy via elastic deformation.

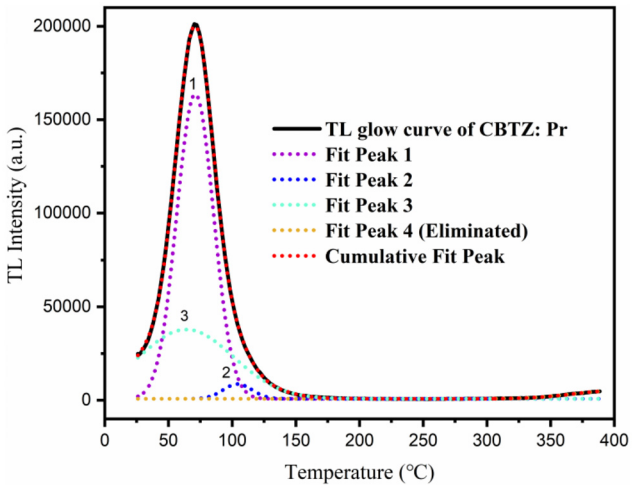

FIG. 3. TL glow curve and multiple Gaussian decomposition.

TABLE I. Frequency factor and theoretical half-lifetime t_*.

	Peak 1	Peak 2	Peak 3
S (s^{-1})	1.053×10^9	4.24×10^{13}	52.08
t_* (s)	583	9860	122

With the activation energy calculated above, another important kinetic parameter, s, which is the frequency factor related to the decay time of thermoluminescence, can be calculated by Eq. (2).[23] Then, the theoretical half-lifetime t_* is estimated by Eq. (3),

$$s = \left[2\beta\left(\frac{1.26T_m}{\omega} - 1\right)\Big/(e^2 T_m)\right]\exp(2.52T_m/\omega)\,, \tag{2}$$

$$t_* = s^{-1}\exp(E/kT)\,, \tag{3}$$

where β is the heating rate of the sample. As a result, the theoretical half-life t_* for different traps are shown in Table I:

Meanwhile, the experimental half-lifetime (t_i) could be directly obtained from the decay curve of persistent luminescence (PsL).[42] As shown in Fig. 4, the experimental half-lifetime (t_i) of CBTZ:Pr is accurately estimated by triple exponential decay fitting the measured PsL decay curve with a triple exponential decay using Eq. (4), where τ_i represents the exponential time constant. Here, the experimental half-lifetime t_i ($t_i = 0.693\tau_i$) is used as a representative of the exponential time constant for convenience of comparing it to the theoretical half-lifetime t_* that is responsible for the traps calculated in the TL glow curve,

$$I = I_0 + I_1 e^{-\frac{t-t_0}{\tau_1}} + I_2 e^{-\frac{t-t_0}{\tau_2}} + I_3 e^{-\frac{t-t_0}{\tau_3}}. \tag{4}$$

Therefore, as presented in Tables I and II, the experimental half-lifetime t_i are generally much shorter than theoretical value t_* deducted from TL glow curve. Intriguingly, this deviation between the calculated value and the practical value conforms to the anomalous fading effect, which indicates the occurrence of the tunneling effect during PsL.[23,43,44] This further proves the existence of geometrically adjacent traps, which is one of the necessary conditions for electron tunneling.

TABLE II. Experimental half-lifetime t_i of CBTZ:Pr.

Decay time constant τ_i	$\tau_1 = 10.73$	$\tau_2 = 37.46$	$\tau_3 = 156.56$
Experimental half-lifetime t_i (s)	$t_1 = 7.44$	$t_2 = 25.96$	$t_3 = 108.50$

Combining the trap depth calculation and anomalous fading effect discovered above, the energy level graph for presenting the EML mechanism model of CBTZ:Pr is constructed (Fig. 5) with each transfer of energy type and position of trap level marked out. The trivalent Pr^{3+} are first excited by irradiation of UV light and free electrons are produced with tetravalent Pr^{4+} (Process I). Most of the free electrons recombine with Pr^{4+} and return to lower levels, emitting red light simultaneously, and this phenomenon is recognized as PL corresponding to the spectrum measured in Fig. 2(a). At the same time, some free electrons are caught by positively charged traps with different depths (Process II). The electrons in traps with the appropriate depth (shallow traps for peak 3) will be gradually released by thermal energy from the ambient environment. The electrons in traps of peaks 2 and 1, which have a higher activation energy, are barely released by thermal energy at room temperature. Therefore, they tend to remain trapped unless the ambient temperature increases in accordance with TL, as measured in Fig. 3.

However, the question lies in how the electrons transfer between different trap levels and luminescent centers. Considering the anomalous fading phenomenon that induced by the tunneling effect in PsL materials discussed above, it is possible to explain the migration of electrons triggered by electron tunneling rather than passing through the conduction band. When traps are more geometrically adjacent to luminescent centers, the possibility of tunneling through the potential barrier will increase. The relationship between the possibility of tunneling P(r) and geometric distance s is shown in the following equation:[45]

$$P(r) = P_0 \exp\left(-\frac{r}{a}\right) = P_0 \exp(-\alpha r)\,. \tag{5}$$

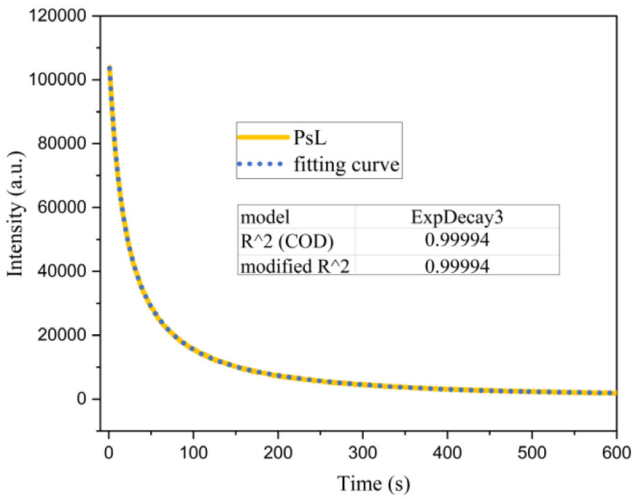

FIG. 4. PsL decay curve of CBTZ:Pr and fitting.

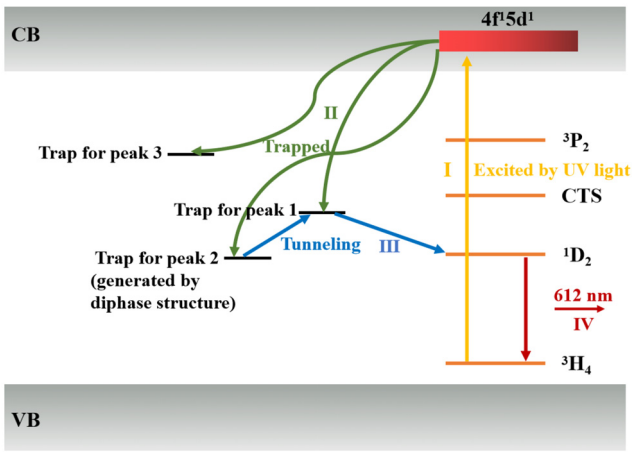

FIG. 5. EML mechanism model for CBTZ:Pr.

When force is applied to the CBTZ:Pr crystal, it undergoes deformation, causing a change in the distance r. As the distance shortens, the probability of tunneling increases, allowing trapped electrons to migrate to the luminescent center without passing through the conduction band. Similarly, the electrons can also migrate between different traps through the tunneling effect. Electrons in deep traps, especially those in peak 2, are difficult to be released by thermal energy at room temperature. However, they can move to adjacent PsL traps or directly to the luminescent centers through the tunneling effect (Process III). After the trapped electrons migrate to the luminescent centers, they recombine with Pr^{4+} ions, subsequently inducing the emission of photons (Process IV).

In conclusion, long-lasting sustainable EML has been observed from non-piezoelectric perovskite CBTZ:Pr consisting of orthorhombic phosphor phase and cubic phase. By analyzing the TL glow curve and PsL behavior, which support the participation of deep traps and origination of anomalous fading effect, a deep trap controlled quantum tunneling model is developed to explain the EML process of CBTZ:Pr. The shortening of the distance between traps and luminescent centers, caused by elastic deformation, increases the possibility of tunneling. This, in turn, transfers the trapped electrons to the luminescent center instead of releasing them into the conduction band. In fact, it is a challenge for many piezoelectric EML materials to manipulate the depth of trap levels since the traps need to be deep enough to keep electrons but shallow enough to be released by piezoelectric field. The model of the deep trap-controlled tunneling mechanism model can offer an approach to developing of non-piezoelectric EML dielectrics, surmounting limitation on screening the EML materials within luminescent ions doped piezoelectric host.

See the supplementary material for more experimental details and results.

This work was supported by the National Natural Science Foundation of China funded by the China Government (No. 12004119).

AUTHOR DECLARATIONS

Conflict of Interest

The authors have no conflicts to disclose.

Author Contributions

Yin Li and Zishuo Li contribute equally to this work.

Yin Li: Data curation (lead); Investigation (lead); Writing – original draft (equal). **Zishuo Li:** Formal analysis (lead); Methodology (equal). **Hailing Sun:** Conceptualization (lead); Methodology (lead); Writing – review & editing (lead). **Kin Wing Kwok:** Project administration (lead); Supervision (lead). **Guofu Zhou:** Conceptualization (equal).

DATA AVAILABILITY

The data that support the findings of this study are available from the corresponding authors upon reasonable request.

REFERENCES

[1]X. D. Wang, H. L. Zhang, R. M. Yu, L. Dong, D. F. Peng, A. H. Zhang, Y. Zhang, H. Liu, C. F. Pan, and Z. L. Wang, "Dynamic pressure mapping of personalized handwriting by a flexible sensor matrix based on the mechanoluminescence process," Adv. Mater. **27**, 2324–2331 (2015).
[2]D. F. Peng, B. Chen, and F. Wang, "Recent advances in doped mechanoluminescent phosphors," Chempluschem **80**, 1209 (2015).
[3]B. Chen, D. F. Peng, P. Lu, Z. P. Sheng, K. Y. Yan, and Y. Fu, "Evaluation of vibration mode shape using a mechanoluminescent sensor," Appl. Phys. Lett. **119**, 094102 (2021).
[4]H. M. Chen, L. Wu, T. Q. Sun, R. Dong, Z. Z. Zheng, Y. F. Kong, Y. Zhang, and J. J. Xu, "Intense green elastico-mechanoluminescence from $KZn(PO_3)_3$:Tb^{3+}," Appl. Phys. Lett. **116**, 051904 (2020).
[5]Y. Y. Du, Y. Jiang, T. Y. Sun, J. X. Zhao, B. L. Huang, D. F. Peng, and F. Wang, "Mechanically excited multicolor luminescence in lanthanide ions," Adv. Mater. **31**, 1807062 (2019).
[6]T. Zheng, M. Runowski, I. R. Martín, K. Soler-Carracedo, L. Peng, M. Skwierczyńska, M. Sójka, J. Barzowska, S. Mahlik, H. Hemmerich, F. Rivera-López, P. Kulpiński, V. Lavín, D. Alonso, and D. F. Peng, "Mechanoluminescence and photoluminescence heterojunction for superior multimode sensing platform of friction, force, pressure, and temperature in fibers and 3D-printed polymers," Adv. Mater. (published online 2023).
[7]Y. C. Ding, B. So, J. K. Cao, and L. Wondraczek, "Ultrasound-induced mechanoluminescence and optical thermometry toward stimulus-responsive materials with simultaneous trigger response and read-out functions," Adv. Sci. **9**, 2201631 (2022).
[8]A. Duval, P. Houizot, X. Rocquefelte, and T. Rouxel, "Mechanoluminescence of (Eu, Ho)-doped oxynitride glass-ceramics from the BaO-SiO_2-Si_3N_4 chemical system," Appl. Phys. Lett. **123**, 011905 (2023).
[9]C. F. Wang, R. H. Ma, D. F. Peng, X. H. Liu, J. Li, B. R. Jin, A. X. Shan, Y. Fu, L. Dong, W. C. Gao, Z. L. Wang, and C. F. Pan, "Mechanoluminescent hybrids from a natural resource for energy-related applications," Infomat **3**, 1272–1284 (2021).
[10]C. N. Xu, T. Watanabe, M. Akiyama, and X. G. Zheng, "Artificial skin to sense mechanical stress by visible light emission," Appl. Phys. Lett. **74**, 1236–1238 (1999).
[11]C. N. Xu, T. Watanabe, M. Akiyama, and X. G. Zheng, "Direct view of stress distribution in solid by mechanoluminescence," Appl. Phys. Lett. **74**, 2414–2416 (1999).
[12]J. C. Zhang, Y. Z. Long, X. Yan, X. S. Wang, and F. Wang, "Creating recoverable mechanoluminescence in piezoelectric calcium niobates through Pr^{3+} doping," Chem. Mater. **28**, 4052–4057 (2016).
[13]S. M. Jeong, S. Song, S. K. Lee, and B. Choi, "Mechanically driven light-generator with high durability," Appl. Phys. Lett. **102**, 051110 (2013).
[14]D. F. Peng, Y. Jiang, B. L. Huang, Y. Y. Du, J. X. Zhao, X. Zhang, R. H. Ma, S. Golovynskyi, B. Chen, and F. Wang, "A ZnS/CaZnOS heterojunction for efficient mechanical-to-optical energy conversion by conduction band offset," Adv. Mater. **32**, 1907747 (2020).
[15]B. P. Chandra, V. K. Chandra, and P. Jha, "Piezoelectrically-induced trap-depth reduction model of elastico-mechanoluminescent materials," Physica B **461**, 38–48 (2015).
[16]B. P. Chandra, V. K. Chandra, and P. Jha, "Microscopic theory of elastico-mechanoluminescent smart materials," Appl. Phys. Lett. **104**, 031102 (2014).
[17]V. K. Chandra, B. P. Chandra, and P. Jha, "Strong luminescence induced by elastic deformation of piezoelectric crystals," Appl. Phys. Lett. **102**, 241105 (2013).
[18]J. C. Zhang, C. N. Xu, S. Kamimura, Y. Terasawa, H. Yamada, and X. S. Wang, "An intense elastico-mechanoluminescence material CaZnOS:Mn^{2+} for sensing and imaging multiple mechanical stresses," Opt. Express **21**, 12976–12986 (2013).
[19]Y. J. Zhao, D. F. Peng, G. X. Bai, Y. Q. Huang, S. Q. Xu, and J. H. Hao, "Multiresponsive emissions in luminescent ions doped quaternary piezophotonic materials for mechanical-to-optical energy conversion and sensing applications," Adv. Funct. Mater. **31**, 2010265 (2021).
[20]A. Baldereschi, "Theory of isoelectronic traps," J. Lumin. **7**, 79–91 (1973).
[21]H. Matsui, C. N. Xu, and H. Tateyama, "Stress-stimulated luminescence from $ZnAl_2O_4$:Mn," Appl. Phys. Lett. **78**, 1068–1070 (2001).
[22]S. Kamimura, H. Yamada, and C. N. Xu, "Development of new elasticoluminescent material $SrMg_2(PO_4)_2$:Eu," J. Lumin. **132**, 526–530 (2012).
[23]R. Chen and S. W. McKeever, *Theory of Thermoluminescence and Related Phenomena* (World Scientific, 1997).
[24]T. Aitasalo, J. Hölsä, H. Jungner, M. Lastusaari, and J. Niittykoski, "Mechanisms of persistent luminescence in Eu^{2+}, RE^{3+} doped alkaline earth aluminates," J. Lumin. **94-95**, 59–63 (2001).

[25]P. Dorenbos, "Mechanism of persistent luminescence in $Sr_2MgSi_2O_7:Eu^{2+}$; Dy^{3+}," Phys. Status Solidi B **242**, R7–R9 (2005).
[26]F. Clabau, X. Rocquefelte, S. Jobic, P. Deniard, M. H. Whangbo, A. Garcia, and T. Le Mercier, "Mechanism of phosphorescence appropriate for the long-lasting phosphors Eu^{2+}-doped $SrAl_2O_4$ with codopants Dy^{3+} and B^{3+}," Chem. Mater. **17**, 3904–3912 (2005).
[27]C. G. Chen, Z. Lin, H. H. Huang, X. Pan, T. L. Zhou, H. D. Luo, L. B. Jin, D. F. Peng, J. Xu, Y. X. Zhuang, and R. J. Xie, "Revealing the intrinsic decay of mechanoluminescence for achieving ultrafast-response stress sensing," Adv. Funct. Mater. (published online 2023).
[28]A. J. Walton, "Triboluminescence," Adv. Phys. **26**, 887–948 (1977).
[29]J. C. Zhang, X. S. Wang, G. Marriott, and C. N. Xu, "Trap-controlled mechanoluminescent materials," Prog. Mater. Sci. **103**, 678–742 (2019).
[30]A. Feng and P. F. Smet, "A review of mechanoluminescence in inorganic solids: Compounds, mechanisms, models and applications," Materials **11**, 484 (2018).
[31]H. F. Zhao, X. S. Wang, X. M. Feng, H. Fang, Y. X. Li, and X. Yao, "Elastico-mechanoluminescence in non-piezoelectric CaTiO3:Pr3+," in *2016 Joint IEEE International Symposium on the Applications of Ferroelectrics, European Conference on Application of Polar Dielectrics, and Piezoelectric Force Microscopy Workshop (ISAF/ECAPD/PFM)* (IEEE, 2016), pp. 1–4.
[32]L. Yang, L. Li, L. X. Cheng, T. T. Jia, F. Hu, S. H. Yu, R. Sun, S. S. Wang, X. F. Shi, and J. C. Zhang, "Intense and recoverable piezoluminescence in Pr^{3+}-activated $CaTiO_3$ with centrosymmetric structure," Appl. Phys. Lett. **118**, 053901 (2021).
[33]J. C. Zhang, Y. Y. Xue, Y. F. Zhu, S. S. Wang, H. W. He, X. Yan, X. Ning, D. Wang, and J. R. Qiu, "Ultra-long-delay sustainable and short-term-friction stable mechanoluminescence in Mn^{2+}-activated $NaCa_2GeO_4F$ with centrosymmetric structure," Chem. Eng. J. **406**, 126798 (2021).
[34]P. Zhang, Z. Z. Zheng, L. Wu, Y. F. Kong, Y. Zhang, and J. J. Xu, "Self-reduction-related defects, long afterglow, and mechanoluminescence in centrosymmetric $Li_2ZnGeO_4:Mn^{2+}$," Inorg. Chem. **60**, 18432–18441 (2021).
[35]Y. Q. Bai, F. Wang, L. Q. Zhang, D. A. Wang, Y. M. Liang, S. R. Yang, and Z. F. Wang, "Interfacial triboelectrification-modulated self-recoverable and thermally stable mechanoluminescence in mixed-anion compounds," Nano Energy **96**, 107075 (2022).
[36]W. Jia, D. Jia, T. Rodriguez, D. R. Evans, R. S. Meltzer, and W. M. Yen, "UV excitation and trapping centers in $CaTiO_3:Pr^{3+}$," J. Lumin. **119–120**, 13–18 (2006).
[37]P. T. Diallo, P. Boutinaud, R. Mahiou, and J. C. Cousseins, "Red luminescence in Pr^{3+}-doped calcium titanates," Phys. Status Solidi A **160**, 255–263 (1997).
[38]M. Zheng, H. L. Sun, M. K. Chan, and K. W. Kwok, "Reversible and nonvolatile tuning of photoluminescence response by electric field for reconfigurable luminescent memory devices," Nano Energy **55**, 22–28 (2019).
[39]H. L. Sun, X. Wu, T. H. Chung, and K. W. Kwok, "In-situ electric field-induced modulation of photoluminescence in Pr-doped $Ba_{0.85}Ca_{0.15}Ti_{0.90}Zr_{0.10}O_3$ lead-free ceramics," Sci. Rep.-Uk. **6**, 28677 (2016).
[40]H. L. Sun, M. C. Wong, G. F. Zhou, and K. W. Kwok, "Tuning electroluminescence performance in Pr-doped piezoelectric bulk ceramics and composites," J. Materiomics **7**, 264–270 (2021).
[41]T. Matsuzawa, Y. Aoki, N. Takeuchi, and Y. Murayama, "A new long phosphorescent phosphor with high brightness, $SrAl_2O_4:Eu^{2+},Dy^{3+}$," J. Electrochem. Soc. **143**, 2670–2673 (1996).
[42]C. Y. Tsai, J. W. Lin, Y. P. Huang, and Y. C. Huang, "Modeling and assessment of long afterglow decay curves," Sci. World J. **2014**, 102524 (2014).
[43]Z. W. Pan, Y. Y. Lu, and F. Liu, "Sunlight-activated long-persistent luminescence in the near-infrared from Cr^{3+}-doped zinc gallogermanates," Nat. Mater. **11**, 58–63 (2012).
[44]E. Uzun, Y. Yarar, and A. N. Yazici, "Electron immigration from shallow traps to deep traps by tunnel mechanism on seydişehir aluminas," J. Lumin. **131**, 2625–2629 (2011).
[45]S. W. S. McKeever, *Thermoluminescence of Solids* (Cambridge University Press, 1985).